ResearchGate

See discussions, stats, and author profiles for this publication at: https://www.researchgate.net/publication/236931348

Ionic Liquids Based on Polynitrile Anions: Hydrophobicity, Low Proton Affinity, and High Radiolytic Resistance Combined

ARTICLE *in* THE JOURNAL OF PHYSICAL CHEMISTRY B · MAY 2013

Impact Factor: 3.3 · DOI: 10.1021/jp404313g · Source: PubMed

CITATIONS
11

READS
26

3 AUTHORS:

Ilya Shkrob
Argonne National Laboratory
143 PUBLICATIONS **2,164** CITATIONS
SEE PROFILE

Timothy W Marin
Benedictine University
54 PUBLICATIONS **810** CITATIONS
SEE PROFILE

James Wishart
Brookhaven National Laboratory
115 PUBLICATIONS **3,642** CITATIONS
SEE PROFILE

Available from: Timothy W Marin
Retrieved on: 27 January 2016

THE JOURNAL OF PHYSICAL CHEMISTRY B

Article

pubs.acs.org/JPCB

Ionic Liquids Based on Polynitrile Anions: Hydrophobicity, Low Proton Affinity, and High Radiolytic Resistance Combined

Ilya A. Shkrob,*[,†] Timothy W. Marin,[†,‡] and James F. Wishart[§]

[†]Chemical Sciences and Engineering Division, Argonne National Laboratory, 9700 S. Cass Ave, Argonne, Illinois 60439, United States

[‡]Chemistry Department, Benedictine University, 5700 College Road, Lisle, Illinois 60532, United States

[§]Chemistry Department, Brookhaven National Laboratory, Upton, New York 11973-5000, United States

Supporting Information

ABSTRACT: Ionic liquids (IL) are being considered as replacements for molecular diluents in spent nuclear fuel reprocessing. This development is hampered by the dearth of constituent anions that combine high hydrophobicity, low metal cation and proton affinity, and radiation resistance. We demonstrate that polynitrile anions have the potential to meet these challenges. Unlike the great majority of organic anions, such polynitrile anions are resistant to oxidative fragmentation during radiolysis, yielding stable N- and C-centered radicals. Moreover, their radical dianions (generated by reduction of the anions) generally undergo protonation in preference to elimination of the cyanide. This is in contrast to fluorinated anions (another large class of anions with low proton affinity), for which radiation-induced release of fluoride is a common occurrence. The "weak spot" of the polynitrile anions appears to be their excited-state dissociation, but at least one of these anions, 1,1,2,3,3-pentacyanopropenide, is shown to resist fragmentation in room temperature radiolysis. We suggest beginning the exploration of ionic liquids based on such polynitrile anions.

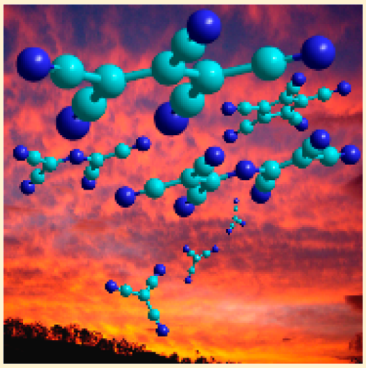

1. INTRODUCTION

Hydrophobic room-temperature ionic liquids (ILs)[1] are currently being considered as replacements for traditional molecular diluents in nuclear cycle separations.[2−12] In the course of spent nuclear fuel reprocessing, the organic solvent remains in contact with aqueous raffinate that contains decaying radionuclides,[2−4] which cause radiolytic damage of the IL solvent. Organic complexes of radionuclide ions are typically extracted into the IL solvent under one set of conditions (e.g., high acidity) and back extracted into the aqueous phase under a different set of conditions (e.g., low acidity).[2,5] As these conditions constantly alternate during the use cycle,[5] the IL needs to remain robust across a wide acidity range; however, ILs vary widely in their resistance to ion exchange and extraction of inorganic acids.[1,2,6]

A particularly vexing problem[6] is the ease of protonation for many of the anions that are used to constitute ILs (C^+A^-) when these liquids are brought into contact with strong aqueous acids (H^+B^-):

$$(C^+A^-)_{IL} + (H^+B^-)_{aq} \rightarrow (C^+B^-)_{IL} + (H^+A^-)_{IL}$$

Such reconstitution, even when it is reversible, alters the chemical composition and physical properties of ILs, and steps would be required to reconstitute the IL during back extraction, which would reduce process efficiency. For this reason, it is highly desirable that the constituent anion (A^-) is a superacid base that cannot be protonated even at high acidity. It is also desirable that the anion is hydrophobic, as otherwise it could exchange with inorganic anions present in the aqueous raffinate. Since the choice of superacids with chemically resistant, hydrophobic conjugate bases is limited, the variety of the constituting IL anions has also been limited, with the bistriflimide (NTf_2^-, where Tf is the triflyl group CF_3SO_2) being the most popular choice. The latter anion exemplifies the typical design of superacids, where the electron withdrawal is promoted through the strategic placement of fluorinated groups.

As the radionuclides decay, they emit ionizing radiation that impinges on the constituent ions of the IL, electronically exciting them and releasing electrons and creating electron deficiencies ("holes"). This ionization/excitation has several chemical consequences. First, it oxidizes the anions by electron detachment. Most of the resulting neutral radicals promptly release inorganic fragments that carry the negative charge in the parent anion (e.g., the oxidized TfO^- dissociates to $^\bullet CF_3$ + SO_3).[7] Second, the released electrons ($e^{\bullet-}$) attach to fluorocarbon groups (see above) releasing fluoride anion (e.g., reduced NTf_2^- dissociates to F^- and $^\bullet CF_2SO_2NTf^-$).[7−10] Third, there is also generation of excited states of the anions that causes dissociation of weak bonds in such states (e.g., NTf_2^{-*} dissociates to $CF_3SO_2^\bullet$ + $TfN^{\bullet-}$).[7,9] In combination, these reactions cause substantial loss of the anions.

Received: May 1, 2013
Revised: May 17, 2013
Published: May 22, 2013

 © 2013 American Chemical Society dx.doi.org/10.1021/jp404313g | J. Phys. Chem. B 2013, 117, 7084−7094

The most detrimental of these reactions is oxidative fragmentation, which precludes the use of many anions. In this regard, the imide anions, such as bistriflimide and dicyanamide (Scheme 1),[9] are exceptional, as their oxidation yields nondissociative imidyl (>N•) radicals.[7,11,12] Such radicals readily abstract H atoms from organic ions, turning into acids (>N$^-$H$^+$),[7,10,12] but these radicals do not dissociate and the anion is recycled. In ref 12, we demonstrated that aromatic imides do not dissociate in their oxidized, reduced, and electronically excited states. However, only one of these imides (1,2-benzenedisulfonimide) had sufficiently low proton affinity (pK_a −1 in water) to avoid protonation in contact with strongly acidic solutions.

Scheme 1. Polynitrile Mono- and Dianions: (a) Dicyanamide (DCA$^-$), (b) Tricyanomethanide (TCM$^-$), (c) Tetracyano-2-azapropenide (TCAP$^-$), (d) 1,1,2,3,3-Pentacyanopropenide (PCP$^-$), (e) 1,1,2,4,5,5-Hexacyano-3-azapentadienide (HCAP$^-$), (f) 1,2,3,4,5-Pentacyanocyclopentadienide (PCCP), (g) 2,3,4,5-Tetracyanocyclopentadienide (TCCP$^{\bullet-}$), (h) 1,2,3-Tris(Dicyanomethylene)Cyclopropanediide (TDCP^{2-}), and (i) 2-Dicyanomethylene-1,1,3,3-tetracyanopropanediide (TCPD^{2-})

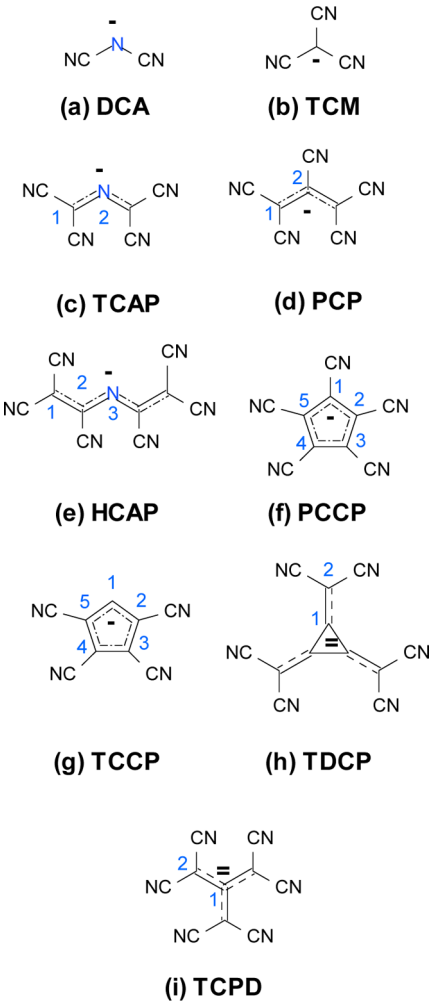

Are there other classes of anions that (i) are sufficiently hydrophobic, (ii) have very low proton affinity, and (iii) are resistant to radiolysis? A brief examination of the known superacids (see, for example, Table 1 in ref 13) reveals that many of these superacids are fluorinated compounds that are prone to F$^-$ loss in their reduced and excited states. There are also untraditional superacids (e.g., carboranes studied by Reed and co-workers)[13] but these compounds, too, tend to involve halogens. Excluding such compounds, there is only one *large* class of anions left: polynitrile compounds (some of which are shown Scheme 1) in which several cyanide groups (often arranged into the dicyanomethylene group, Q) have the same electron-withdrawing function as the triflyl groups in fluoro compounds. In particular, the dicyanomethylene group is electronically analogous to oxygen,[15] so that TCAP$^-$ (Scheme 1) and TCPD^{2-} (Scheme 1) are the polynitrile analogs of the familiar nitrate and carbonate anions.

ILs containing the tetracyanoborate (B(CN)$_4^-$), dicyanamide, and tricyanomethanide anions (DCA$^-$, TCM$^-$, Scheme 1) are well-known,[16,17] and their low viscosities and high conductivities make them useful in solar photochemical cells.[18] For a given cation, IL hydrophobicity increases with the number of cyano groups in the anion. Our previous studies indicated good radiation stability of dicyanamide ILs but fragmentation of the tetracyanoborates by reductive and oxidative mechanisms.[7,9−11] However, more complex polynitrile anions have so far escaped attention of the IL community (with one exception),[19] and we sought to bridge this gap. To this end, we present several methods for synthesis of ionic compounds based on such anions (see section 1S in the Supporting Information)[20−22] and we assess their radiation stability using spectroscopic and analytical methods. Some of these polynitrile anions actually have *lower* proton affinity than the more common fluorinated anions.[14,23] For example, the pK_a (in acetonitrile) of the conjugate acid of PCP$^-$ (Scheme 1) is −2.8, which is considerably lower than 1.8 for BF$_4^-$, 0.7 for TfO$^-$, 0.3 for NTf$_2^-$, and −1.0 for B(CN)$_4^-$.[14] In 1,2-dichloroethane, the pK_a for this acid is comparable to that of Tf$_3$CH (−15.3 versus −16.4), which is one of the strongest acids known. The reasons to anticipate radiation stability of such polynitrile anions present themselves by their structure. One-electron oxidation of DCA$^-$, TCAP$^-$, and HCAP$^-$ (Scheme 1) yields stable imidyl radicals that are analogous to the •NTf$_2$ radical observed in irradiated bistriflimide compounds.[7,9,12] One-electron oxidation of TCM$^-$ (Scheme 1) yields tricyanomethyl radical, •C(CN)$_3$, which is not known to dissociate (as it typically decays by cross recombination in solution).[24,25] Analogous C-centered p-radicals can be expected for PCP$^-$ and PCCP$^-$ (Scheme 1). For PCP$^-$, not only this *neutral* p-radical would be stable; a stable electron adduct, PCP$^{\bullet 2-}$, has been obtained by Li^0 reduction of PCP$^-$ in tetrahydrofuran,[26] indicating that this anion does not readily eliminate cyanide when it is reduced.

The paper is organized as follows. Synthetic and experimental methods are discussed in section 2. The structural considerations articulated above are substantiated in section 3 using density functional theory (DFT) calculations. Electron paramagnetic resonance (EPR) spectroscopy of irradiated polynitrile anion compounds is examined in section 4.1, and product analyses using mass spectrometry (MS) and nuclear magnetic resonance (NMR) are given in section 4.2. The summary of these results and their practical import are given in section 5. To save space, the methods, supporting tables and figures, and list of abbreviations are placed in the Supporting Information. When referenced in the text, these materials have the designator "S", as in Figure 1S.

dx.doi.org/10.1021/jp404313g | J. Phys. Chem. B 2013, 117, 7084−7094

2. EXPERIMENTAL AND COMPUTATIONAL METHODS

Unless specified otherwise, all reagents were obtained from Aldrich and used as supplied without further purification. The details of synthetic procedures (section 1S), melting points for solid compounds (Table 1S), mass peaks for ions (Table 2S) and fragmentation pathways for anions (Table 3S), and nuclear magnetic resonance (NMR) data (Table 4S) are given in the Supporting Information. For tetra(*n*-alkyl)ammonium (N_{abcd}^+) and phosphonium (P_{abcd}^+) cations, indices (*a*–*d*) indicate the carbon number in the alkyl arms of the cation; $PyBz^+$ stands for 1-benzylpyridinium and $mimBz^+$ for 1-benzyl-3-methylimidazolium. Tricyanomethanide compounds were obtained using K TCM supplied by Alfa Aesar that was purified by treating the aqueous solution with activated charcoal (section 1S.1). $[N_{4444}]_2$ TDCP, K TCCP, and N_{2222} PCCP were a generous gift of Prof. Joel S. Miller (University of Utah).

For product analyses, nitrogen-purged samples were placed in sealed, water-cooled NMR tubes (o.d. 5 mm) and irradiated by 2.5 MeV electrons to a total dose of 2–4 MGy using a dose rate of 6.8 kGy/s (1 Gy = 1 J/kg of the absorbed energy). ^{13}C NMR spectra were obtained in dimethyl sulfoxide-d_6 (DMSO-d_6), using an Avance DMX 500-MHz spectrometer (Bruker); the chemical shifts are given versus tetramethylsilane (TMS). Tandem electrospray ionization mass spectra (ESI MS_n) were obtained using a Thermo Scientific LCQ Fleet ion trap mass spectrometer operating either in positive or negative modes ($MS_n^{\pm}$). MS_1 corresponds to the first quadrupole and MS_2 corresponds to collision-induced dissociation (of mass-selected ions) modes of operation. Liquid samples were injected directly into the ion trap in dilute acetonitrile solutions.

For EPR spectroscopy, solid or liquid samples placed in Suprasil tubes were frozen by rapid immersion in liquid nitrogen and irradiated to 3 kGy at 77 K. The radicals were observed using a 9.44 GHz Bruker ESP300E spectrometer, with the sample tube placed in a flow helium cryostat (Oxford Instruments CF935). The magnetic field **B** and the hyperfine coupling constants (hfcc's) are given in the units of gauss (1 G = 10^{-4} T). If not stated otherwise, the first-derivative EPR spectra were obtained at 50 K using 2 G modulation at 100 kHz. The radiation-induced EPR signal from the E'_γ center in the Suprasil sample tubes (that frequently overlapped with the resonance lines of organic radicals) is shadowed in the EPR spectra given in the figures.

The calculations of the hfcc's and radical structures were carried out using a density functional theory (DFT) method with the B3LYP functional[27] and 6-31+G(d,p) basis set from Gaussian 03.[28] In the following, a_{iso} denotes the isotropic hfcc and *B* the anisotropic part of the hfc tensor ***A*** with the principal axes (*a*,*b*,*c*). Powder EPR spectra were simulated using first-order perturbation theory. For convenience, the principal values of the ***g***-tensor are reported as $\delta g_{\nu\nu} = (g_{\nu\nu} - 2 \times 1) \times 10^4$, where $\nu = x,y,z$ are the principal axes of this tensor.

3. PRELIMINARY CONSIDERATIONS

A particular concern with the polynitrile anions (ZCN^-, Scheme 2) is that their reduction can cause CN^- elimination, in analogy to the F^- loss in the reduction of fluorinated anions (section 1). Of the cyano compounds examined in our previous studies,[7,11] it appears that there is no reduction of the DCA^- anions, but $B(CN)_4^-$ anions were readily reduced with subsequent loss of CN^-. As the electron affinity increases for larger polynitrile anions, such concerns become more relevant.

Scheme 2. Main Reduction Pathways for a Generic Polynitrile Anion (ZCN^-)

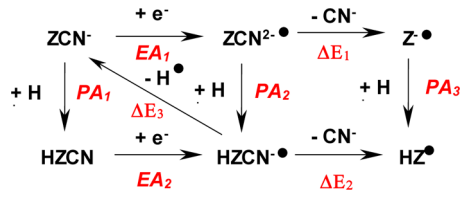

Indeed, these anions may have positive electron affinity in the condensed phase, forming $ZCN^{\bullet 2-}$ radical dianions. The latter can either abstract a proton from the nearby organic cation (as was observed for aromatic imides),[12] forming an $HZCN^{\bullet -}$ radical anion, or dissociate to CN^- and $Z^{\bullet -}$. In turn, the $Z^{\bullet -}$ radical anion can be protonated to yield the neutral $HZ^\bullet$ radical, which can also form by CN^- loss from the protonated form of the radical dianion, that is, $HZCN^{\bullet -}$. This species can also be regarded as the product of H atom addition to the parent anion; in the following, it is referred to as an H atom adduct. Scheme 2 summarizes these transformations and Table 1 gives DFT estimates for adiabatic electron and proton affinities and the corresponding dissociation energies. The optimized geometries, hfcc tensors, and energetics are summarized in Tables 5S and 6S in the Supporting Information.

For TCM^-, the H atom can only add to the cyanide,[29] forming *trans*-$QC^-(H)=N^\bullet$ (in the following, *cis*- and *trans*- refer to the conformation of the proton or dangling bond with respect to a cyanide group or unpaired electrons on nitrogen). For $TCAP^-$ and $HCAP^-$, the $\rangle NH^{\bullet -}$ form of the H atom adduct is preferred in the gas phase, while for PCP^- and $PCCP^-$ addition to carbon-1 is preferred. The DFT calculations indicate that the energetically preferred site for CN^- loss from $HZCN^{\bullet -}$ is from carbon-2 for PCP^- and $HCAP^-$. The corresponding lowest-energy $HZ^\bullet$ radicals are protonated in *trans*-conformation at carbon-1 site. The electron detachment energies increase in the opposite direction, suggesting that the corresponding $ZCN^\bullet$ radicals are strong oxidizers. The preferred mode for oxidation is likely to be proton-coupled electron transfer

$$SH + ZCN^\bullet \rightarrow S^\bullet + H^+ZCN^-$$

where SH is an H-donating organic substrate (such as the IL cation). The gas-phase electron affinity for polynitrile anions is negative, with the highest electron affinity for $HCAP^-$ and the lowest for DCA^- (Table 1). While it is difficult to reliably estimate the polarization energy of these ions in the IL, it is probably ~2–3 eV (as can be roughly estimated from the Born equation), so it is likely that the radical dianion $ZCN^{\bullet 2-}$ is metastable for TCAP, HCAP, PCP, and PCCP. Cyanide elimination from $ZCN^{\bullet 2-}$ is exergonic for DCA, TCM, and TCAP, but it becomes weakly endergonic (or nearly thermoneutral) for HCAP, PCP, and PCCP. As the proton affinity of $ZCN^{\bullet 2-}$ is high, cyanide loss always competes with the protonation. The cyanide in the $HZCN^{\bullet -}$ anion is bound by 1.5–3.5 eV; i.e., this elimination cannot occur in this protonated state. Direct H atom addition to the parent anion is always exergonic. These considerations imply that observation of $HZ^\bullet$ and $Z^{\bullet -}$ radicals is indicative of poor stability of $ZCN^{\bullet 2-}$; if the protonation occurs more rapidly than the dissociation, the resulting $HZCN^{\bullet -}$ radical anion does not subsequently dissociate.

dx.doi.org/10.1021/jp404313g | J. Phys. Chem. B 2013, 117, 7084–7094

Table 1. Energetics for Chemical Reactions Shown in Scheme 2[a]

anion	EDE[b]	EA_1[c]	EA_2[c]	ΔE_1[d]	ΔE_2[d]	ΔE_3[d]	PA_1[e]	PA_2[e]	PA_3[e]
$N(CN)_2^-$[f]	4.06	−4.76	+1.41	−3.20	+1.52	+1.24	13.45	19.62	14.90
$C(CN)_3^-$[f]	4.02	−4.28	+1.94	−2.50	+1.70	+1.39	13.06	19.28	15.07
NQ_2^-	4.57	−2.46	+3.03	−1.28	+2.51	+1.84	12.41	17.91	14.11
$N[C(CN)Q]_2^-$	5.15	−0.49	+3.58	+0.33	+3.42	+2.31	12.33	16.40	13.30
$NCCQ_2^-$	4.78	−1.68	+3.37	−0.28	+2.79	+1.95	12.19	17.24	14.17
$C_5(CN)_5^-$	5.55	−2.26	+3.49	+0.03	+3.21	+1.27	11.39	17.13	13.95

[a]All energies are in eV for gas-phase species as estimated using the B3LYP/6-31+G(d,p) method. [b]Adiabatic electron detachment energy. [c]Adiabatic electron affinity. [d]See Scheme 2. [e]Adiabatic proton affinity. [f]$HZCN^{\bullet-}$ are $-CH{=}N^{\bullet}$ adducts.

We stress that the preferred form of the trapped-hole center is not necessarily the $ZCN^{\bullet}$ radical, as discussed above. Indeed, this radical can share negative charge with the parent anion, forming the $(ZCN)_2^{\bullet-}$ dimer anion with a weak $\sigma^1\sigma^{*2}$ bond. Such hemicolligation is known to occur in halide and pseudohalide anions, and we demonstrated its occurrence for DCA^-.[11] Our DFT calculations indicate that, in the gas phase, the $^{\bullet}C(CN)_3$ radical derived from TCM^- can form a D_{3d} symmetrical $C_2(CN)_6^{\bullet-}$ dimer anion (that is, the radical anion of hexacyanoethane) with the C−C distance of 3.1 Å and binding energy of ∼0.75 eV. These DFT calculations also indicate that such N−N and C−C binding is endergonic for larger polynitrile anions due to steric hindrance in such anions.

Importantly, the dissociation of the anions can proceed not only from their redox states but also from their electronically excited states. For some anions (DCA^-, TCM^-, and $PCCP^-$) such fragmentation is less of a concern, whereas for other ions ($TCAP^-$, PCP^-, and $HCAP^-$) mass spectrometry indicates a common degradation path in which the collisionally activated anion eliminates cyanogen, C_2N_2 (Table 3S): the $TCAP^-$ yields QNC^-, the PCP^- yields $QC{\equiv}CCN^-$, and the $HCAP^-$ yields $QC(CN)NC{\equiv}CCN^-$ anion that further fragments to TCM^- and dicyanoacetylene. The corresponding reaction barriers are fairly low (1.7−2.2 eV, see Table 3S), suggesting that such reactions can occur in the IL. As the diamagnetic species are silent in EPR spectroscopy, only product analysis (section 4.2) can reveal the extent of radiolytic damage through such reaction channels.

Using the DFT estimates for hfcc's in ^{14}N and ^1H nuclei coupled to the unpaired electron, we simulated first-order EPR spectra for many of the radicals that are expected to occur in ILs composed of polynitrile anions. These simulations and structures for the radicals are presented in Figures 1S−12S and will be referred to in section 4.1 as a means to recognize these radical species.

4. RESULTS AND DISCUSSION

4.1. EPR Spectroscopy of Frozen Samples. We start our examination with TCM^- (Scheme 1) proceeding in the order of increased structural complexity. Since radicals derived from organic ions complicate the interpretation of EPR spectra, we have used simpler reference systems (such as alkali and ammonia salts) where possible. In more than one instance, radical attributions were ambiguous. Our goal in this study is less to catalog and interpret all of the observed features in the EPR spectra than to establish the occurrence of fragmentation in reduced polynitrile anions, as such decomposition implies that the corresponding IL diluents are undesirable for use in high radiation fields. We sought to eliminate those anion candidates for which such fragmentation is observed.

4.1.1. TCM^- (Tricyanomethanide). Figure 1a exhibits the first-derivative EPR spectrum obtained for irradiated potassium tricyanomethanide recrystallized from water. This is a composite EPR spectrum, as demonstrated by gradual warming of the sample. After warming to 300 K, the EPR spectrum of this sample transforms into a multiplet resulting from a radical with six equivalent ^{14}N nuclei with $A_{cc} \approx 5.4$ G and $A_{aa,bb} \approx 0$ that has a nearly spherical g-tensor (Figure 1b). This species cannot be the tricyanomethyl radical (see Figures 3S and 13S). The refinement of the magnetic parameters gives $A[^{14}N]$ = (0,0.2,5.2) G (Table 2) versus $A[^{14}N]$ = (−0.4,0.1,5.2) G that was estimated for $C_2(CN)_6^{\bullet-}$. This EPR spectrum is from the $\sigma^1\sigma^{*2}$ dimer radical anion of TCM^- discussed in section 3. Since for every trapped-hole center, such as $C_2(CN)_6^{\bullet-}$, there is a complementary trapped-electron center (due to overall charge neutrality in the sample), it is expected that the interfering resonance lines observed at 50 K belong to a

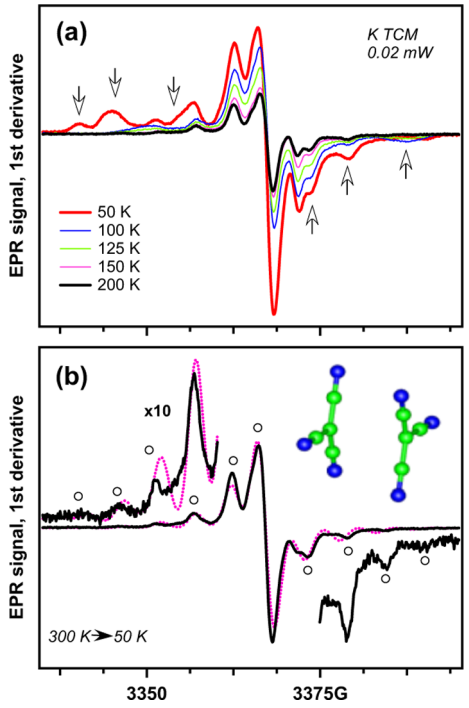

Figure 1. (a) First-derivative EPR spectra of irradiated K TCM:H_2O. As the sample temperature increases, the resonance lines from a trapped-electron center indicated by the arrows decay. (b) EPR spectrum of the same sample warmed to 300 K after cooling back to 50 K (solid line). Only the features from $C_2(CN)_6^{\bullet-}$ (shown in the inset) persist above 200 K. The resonance lines of this trapped-hole center are indicated by the open circles, and the dotted line indicates the best fit using the parameters given in Table 2.

dx.doi.org/10.1021/jp404313g | J. Phys. Chem. B 2013, 117, 7084−7094

Table 2. *g* and Hfcc Tensor Parameters for Selected Radicals Derived from the Polynitrile Anions[a]

attribution	(δg_{XX}, δg_{YY}, δg_{ZZ})	a_{iso} (B_{aa}, B_{bb}, B_{cc}), G
$C_2(CN)_6^{\bullet -}$ [b]	(37.4, 35.5, 32.8)	6 ^{14}N 1.8 (1.8, −1.6, 3.4)
$HC^{\bullet}(CN)_2$ set I[c]	(70.4, 22.8, 38.5)	^{14}N 6.2 (−4.4, −1.4, 5.8)
		^{14}N 7.5 (−0.9, −6.4, 7.3)
		^{1}H −11.0 (−3.0, −6.9, 9.8)
$HC^{\bullet}(CN)_2$ set II[c]	(84.6, 29.0, 39.2)	2 ^{14}N 7.1 (−5.5, −1.0, 6.5)
		^{1}H −11.3 (−1.6, −5.6, 7.4)
$QNCH(CN)_2^{\bullet -}$ [d]	(36.7, 44.0, 40.2)	$^{14}N_Q$ 2.4 (−3.2, −0.7, 3.9)
		$^{14}N_Q$ 0.6 (−3.4, −1.1, 4.4)
		$^{14}N_2$ 6.8 (−7.9, −6.5, 14.3)
QC(CN)NC(CN) $CH(CN)_2^{\bullet -}$ [e]	≈37	3 ^{14}N 1.8 (−1.8, −1.8, 3.6)

[a]The hfcc tensor axes are the same as those given in Table 6S in the Supporting Information. These estimates can be compared with the DFT estimates given in Table 6S. [b]D_{3d} symmetry, *y*-axis of the *g*-tensor is the long axis of the anion shown in Figure 1b. [c]See Figure 14S in the Supporting Information. [d]See Figures 3 (trace ii) and Figure 16S in the Supporting Information. [e]Structure ii in Figure 6.

trapped *electron* center. The comparison with EPR simulations given in Figure 3S suggests that this center cannot be the H atom adduct ($QCHN^{\bullet -}$), which has large proton hfcc of ∼73 G. As was argued in section 3, nonobservation of the H atom adduct is indicative of the cyanide elimination. The only species in Figure 3S that can exhibit an EPR spectrum similar to the one shown in Figure 1a is the $HZ^{\bullet}$ radical (the known nitrile radicals, such as $^{\bullet}CN$ and $C_2N_2^{\bullet -}$, are excluded by comparison to their known spectroscopic features). This EPR spectrum can be simulated assuming either two equivalent cyanide groups or an asymmetrically distorted $HC^{\bullet}(CN)_2$ radical (Table 2, sets I and II). An example of such a simulation is given in Figure 14S. These simulations give the estimates of $a_{iso}(^1H) \sim -11$ G and $a_{iso}(^{14}N) \sim (6-7)$ G versus −19.4 and 4 G for the $HC^{\bullet}(CN)_2$ radical in the gas phase (according to our DFT calculation). The *g*-tensor is strongly asymmetrical (Table 2), suggesting the distortion of the radical in the crystal lattice. In the C_s symmetrical gas-phase structure, in which the hydrogen of $HC^{\bullet}(CN)_2$ forms a weak bond with the cyanide group of the TCM^-, the hfcc on the proton is 10% smaller, and the reduction of $a_{iso}(^1H)$ can be due to more extensive charge sharing. In the gas phase, the $\{H(CN)_2C\cdots C(CN)_3\}^{\bullet -}$ formation is energetically prohibitive (as opposed to the $C_2(CN)_6^{\bullet -}$ formation), but this may not be the case in the solid matrix.

Figure 2a exhibits EPR spectra obtained from the irradiated $P_{666,14}$ TCM. There is a narrow, saturable line at the center of the EPR spectrum that we attribute to the unresolved $C_2(CN)_6^{\bullet -}$ radical anion (see Figure 2b for the comparison of spectral envelopes). There are also several resonance lines from H loss radicals in the aliphatic arms of the cation (that will be referred to as $C(-H)^{\bullet +}$ radicals) that are also observed in other irradiated compounds of $P_{666,14}^+$. In $P_{666,14}$ Cl, only these alkyl radicals are observed (Figure 2a, trace (iii)), and by comparison of the two EPR spectra it is observed that there are resonance lines of a trapped-electron center superimposed on those from the $C(-H)^{\bullet +}$ radicals. The spectral signature of these lines is very similar to the one observed in K TCM

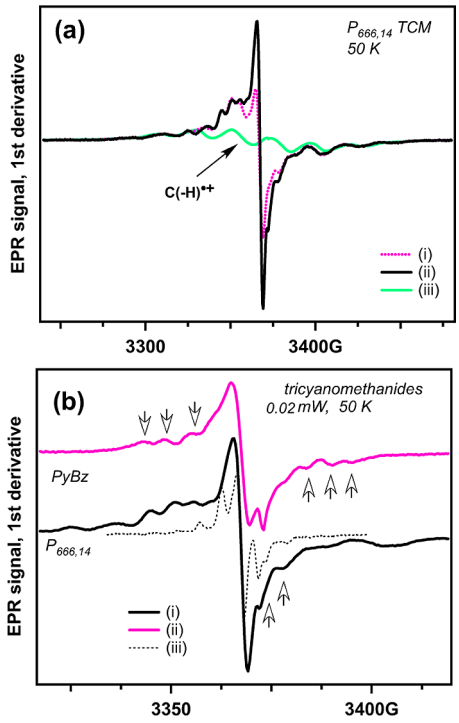

Figure 2. (a) First-derivative EPR spectra of frozen $P_{666,14}$ TCM irradiated at 77 K and observed at 50 K using a microwave power of 2 mW (trace i) and 0.02 mW (trace ii). Trace iii indicates the EPR spectrum of the $C(-H)^{\bullet +}$ radicals derived from the parent cation as observed in irradiated $P_{666,14}$ Cl. (b) The EPR spectra from irradiated $P_{666,14}$ TCM (trace i) and PyBz TCM (trace ii) observed at 50 K compared to the EPR spectrum from $C_2(CN)_6^{\bullet -}$ as observed in irradiated K TCM at 300 K (trace iii). The resonance lines from the electron center are indicated by the arrows. It is seen from this plot and Figure 1a that the same radical species occurs in all three of the tricyanomethanide compounds.

(Figure 1a). The same resonance lines (marked with arrow in the plot) were also observed in irradiated PyBz TCM (Figure 2b); in all three cases, we attribute these resonance lines to the same $HZ^{\bullet}$ radical. While this attribution remains tentative given the discrepancy between the estimated parameters and DFT model of the spin center, it is clear that reduced tricyanomethanide eliminates cyanide, and so the corresponding ILs are not radiation resistant.

4.1.2. $TCAP^-$ (Tetracyano-2-azapropenide). Figure 15S(a) exhibits the EPR spectrum obtained in irradiated crystalline N_{1111} TCAP at 50 K. The two side lines separated by 60 G (that are indicated by arrows in the plot) are almost identical to the same features observed in irradiated $P_{666,14}$ TCAP (a frozen ionic liquid, see Figure 3 and Figure 15S(b)). When $P_{666,14}$ TCAP is warmed to 175 K, the interfering $C(-H)^{\bullet +}$ radicals decay, and this feature (the outer resonance lines of a triplet) is clearly observed (Figure 3). Comparison with the EPR spectra simulated in Figure 4S suggests that this feature stems from the radical dianion, $NQ_2^{\bullet 2-}$ (trace i in Figure 3) which has large hfcc ($A_{zz}[^{14}N] \sim 28$ G) in nitrogen-2. Further warming of the sample to 200 K causes the abrupt change of this EPR spectrum to the one shown at the top of Figure 3 that strongly resembles the EPR spectrum predicted for an H adduct of TCAP, that is, $QNCH(CN)_2^{\bullet -}$ (trace ii in Figure 3). The EPR spectrum of this H adduct is quite different from that of $HNQ_2^{\bullet -}$ (Figure 4S). In the gas phase, $QNCH(CN)_2^{\bullet -}$ is 165 meV more energetic than $HNQ_2^{\bullet -}$ (Table 5S); apparently, these

dx.doi.org/10.1021/jp404313g | J. Phys. Chem. B 2013, 117, 7084−7094

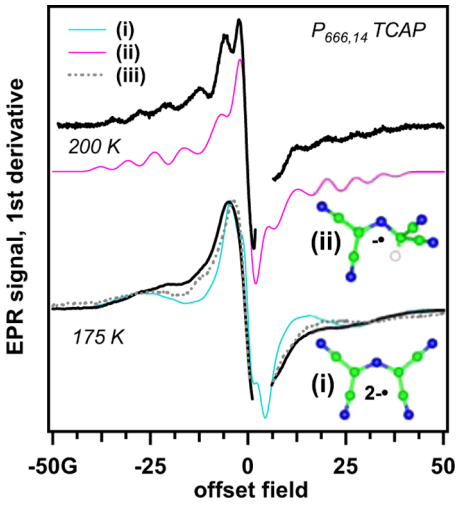

Figure 3. First-derivative EPR spectra observed from $P_{666,14}$ TCAP irradiated at 77 K and observed at 175 K (at the bottom) and 200 K (at the top) at a low microwave power of 0.02 mW. The dashed line (trace iii) is the EPR spectrum observed in irradiated N_{1111} TCAP at 50 K. Traces i and ii are simulated EPR spectra of $NQ_2^{\bullet 2-}$ and QNCH(CN) $^{\bullet -}$ radicals shown in the inset, using the hfcc parameters estimated from our DFT calculations and assuming a spherically symmetrical *g*-tensor (see Figures 4S and Table 6S in the Supporting Information). This parameter set is refined in Table 2 (see Figure 16S).

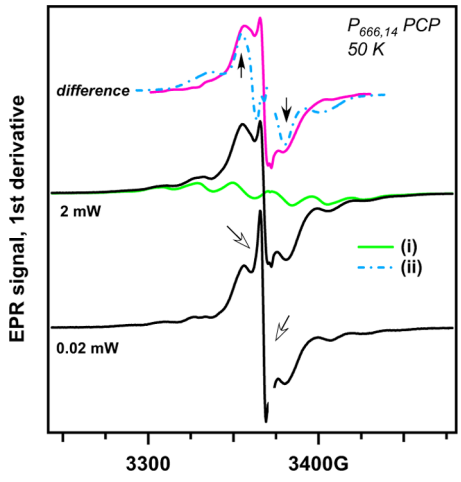

Figure 4. First-derivative EPR spectra observed in irradiated $P_{666,14}$ PCP at 0.02 mW and 2 mW, as indicated in the plot. The arrows indicate the narrow, saturable line at the center. Trace i is the EPR spectrum of the C(−H)$^{\bullet +}$ radicals observed in irradiated $P_{666,14}$ Cl. The difference plot (in which this contribution has been removed) is shown at the top of the plot. Trace ii is the EPR spectrum observed in irradiated N_{1111} PCP at 50 K. The arrows indicate features attributed to the corresponding HZ$^{\bullet}$ radical (see Figure 5 and Figure 6S).

energetics reverse in the solid matrix. Refinement of hfcc parameters (see Figure 16S) gives $A_{zz}[^{14}N]$ of 7.4 and 7.8 G for two cyanide nitrogens and 22 G for nitrogen-2 (where axis *z* is perpendicular to the mirror plane of the radical anion, Table 2) versus the estimated hfcc's of 6.3, 7.5, and 23.8 G, respectively. At lower temperature, there is much interference from the C(−H)$^{\bullet +}$ radicals, but there is also a narrow, saturable resonance line resembling the one observed in N_{1111} TCAP that is likely to originate from the $^{\bullet}NQ_2$ radical (Figure 15S). Such narrow, saturable lines have been observed for other trapped-hole centers in polynitrile compounds (see below), in accord with the simulations shown in Figure 1S.

These results indicate that the reduced $TCAP^-$ anion is remarkably stable. It does not dissociate yielding cyanide; instead, at higher temperature (when the protons become more mobile) this radical dianion undergoes protonation.

4.1.3. PCP$^-$ (1,1,2,3,3-Pentacyanopropenide). Figure 4 and Figure 17S(a) exhibit EPR spectra for irradiated $P_{666,14}$ PCP at 50 K. In addition to the familiar sextet of resonance lines from the C(−H)$^{\bullet +}$ radicals (trace i in Figure 4), there is a narrow, saturable singlet indicated by the open arrows and another broader feature overlapping with this narrow line. After prolonged isothermal annealing at 77 K, this narrow line becomes weaker, suggesting slow radical decay (Figure 17S(a)). This narrow line may belong to $NCC^{\bullet}Q_2$ ($PCP^{\bullet}$) or $PCP^{\bullet 2-}$ radicals that have similar EPR spectra (Figure 1S). The C(−H)$^{\bullet +}$ radicals decay above 175 K (Figure 17S(b)), and the resulting EPR spectrum is shown in Figure 18S. As suggested by microwave power dependence, this is a composite EPR spectrum. The comparison of these EPR spectra with the EPR spectra of HZ$^{\bullet}$ and Z$^{\bullet -}$ radicals in Figure 6S excludes such CN^- loss radicals as progenitors of the observed features. The EPR spectrum obtained at high microwave power best corresponds to the one predicted for an H atom adduct at carbon-2, that is, the $HC(CN)Q_2^{\bullet -}$ radical, whereas the EPR spectrum obtained at low microwave power is more consistent with an H adduct at carbon-1, that is, the QC(CN)CH(CN) $^{\bullet -}$ radical. In the gas phase, the latter species is only 200 meV less energetic than the carbon-2 adduct. (Figure 7S and Table 5S). It is difficult to choose between these two structures, because the spacing of the resonance lines is similar in both of these isomers, and more than one radical isomer can be present in the sample. By analogy to $TCAP^-$ and $HCAP^-$, it is likely that the preferred form is the carbon-1 adduct.

A closer look at Figure 4 reveals a feature indicated by filled arrows; this feature becomes more apparent when the underlying signal from C(−H)$^{\bullet +}$ radicals is subtracted from the spectrum (see the top of Figure 4). This feature resembles the analogous features that are observed in the EPR spectra of irradiated (crystalline) PyBz PCP and N_{1111} PCP after annealing of these samples at 300 K (Figure 5). These features indicate a strong coupling to a single proton in the progenitor, and are best explained by an HZ$^{\bullet}$ radical at carbon-1. It seems, therefore, that $PCP^{\bullet 2-}$ can either (i) eliminate the cyanide with the subsequent protonation of the radical anion or (ii) protonate. This is likely to be due to the relative inefficiency of protonation in a low temperature matrix, as the migration of the protons is inhibited at this temperature. As a result, the radical dianion persists longer, which gives it the opportunity to eliminate the cyanide. While the latter reaction prevails in a frozen matrix, its occurrence in a room temperature IL is not a given, as the $PCP^{\bullet 2-}$ can be protonated faster than it decomposes.

4.1.4. HCAP$^-$ (1,1,2,4,5,5-Hexacyano-3-azapentadienide). As it is possible to obtain the ammonium salt of $HCAP^-$, one can observe radicals derived from this anion without interference from the radical derived from organic cations. Figure 6 exhibits the EPR spectrum of NH_4 HCAP, which does not evolve further upon warming to 300 K (Figure 19S), indicating the exceptional stability of this radical in the crystalline matrix. The septet of the resonance line is definitely from the H adduct to carbon-1 of the parent anion (structure ii in Figure 9S), with three nearly magnetically equivalent ^{14}N

dx.doi.org/10.1021/jp404313g | J. Phys. Chem. B 2013, 117, 7084−7094

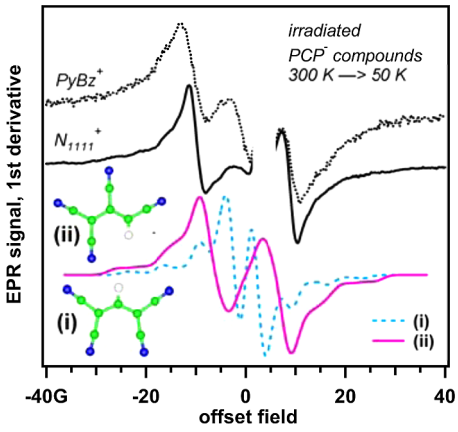

Figure 5. First-derivative EPR spectra observed in crystalline PyBz PCP and N_{1111} PCP that were irradiated at 77 K, warmed to 300 K, and then cooled back to 50 K (0.02 mW). Given at the bottom are simulated EPR spectra of $HZ^{\bullet}$ radicals centered at carbon-2 (trace i) and carbon-1 (trace ii) that were simulated using the hfcc parameters given in Table 6S in the Supporting Information, assuming a spherical *g*-tensor.

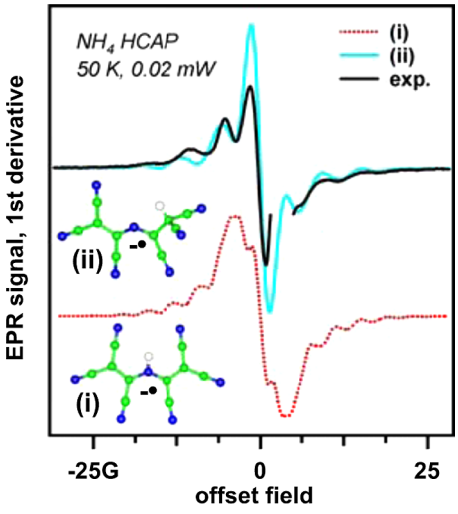

Figure 6. First-derivative EPR spectra observed from irradiated crystalline NH_4 HCAP (solid black line) at 50 K. Traces i and ii are the EPR spectra simulated for H adducts at nitrogen-3 and carbon-1 using the hfcc parameters given in Table 6S in the Supporting Information (assuming a spherical *g*-tensor). The optimized structures of these radicals are given in the insets in the plot.

nuclei (Table 2 and Figure 6 and Figure 8S). In the gas phase, this H adduct is 70 meV more energetic (Table 5S) than the nitrogen-3 adduct (structure i in Figure 9S) which has quite a different EPR spectrum (Figure 6, trace i), but once again protonation at the terminal carbon is preferred in the solid matrix.

In the EPR spectra obtained from N_{4444} HCAP (Figure 20S(a)) and $P_{666,14}$ PCP (Figure 7), there is significant background from the $C(-H)^{\bullet+}$ radicals, but there is also a narrow, saturable signal resembling the trapped-hole centers in other polynitrile systems. The envelope of this line (with the peak-to-peak interval $\Delta B_{pp} \sim 5$ G) is similar to the one observed for H atom adduct, and the radical persists to 200 K (Figures 20S(b) and 21S(a)). This resonance line originates either from the H atom adduct or it is a superposition of contributions from this adduct and $HCAP^{\bullet}$ or $HCAP^{\bullet 2-}$

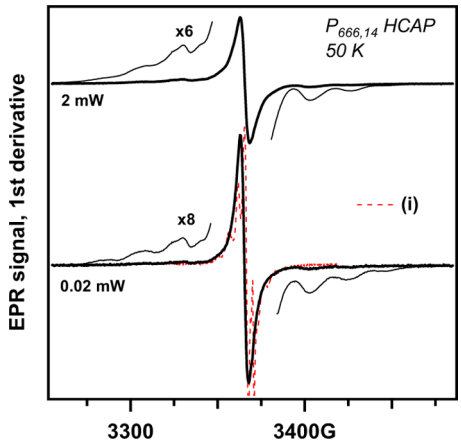

Figure 7. First-derivative EPR spectra observed at 50 K from $P_{666,14}$ HCAP at 0.02 mW and 2 mW, as indicated in the plot. Trace i is the EPR spectrum of the H adduct of $HCAP^{-}$ that is reproduced from Figure 6.

(which have nearly identical EPR spectra, as suggested by simulations shown in Figure 1S). The latter possibility is suggested by the disparity in the doubly integrated EPR signals from the $C(-H)^{\bullet+}$ radicals (which are trapped-hole species) and the narrow line in Figure 7 and Figure 21S(b), suggesting that the progenitors of this line cannot all be trapped-electron species. The presence of $HCAP^{\bullet}$ rationalizes this disparity, and similar trapped-hole centers were observed in other ionic compounds composed of the polynitrile anions.

4.1.5. PCCP⁻ (1,2,3,4,5-Pentacyanocyclopentadienide). Figure 8 exhibits the EPR spectrum of irradiated N_{2222}

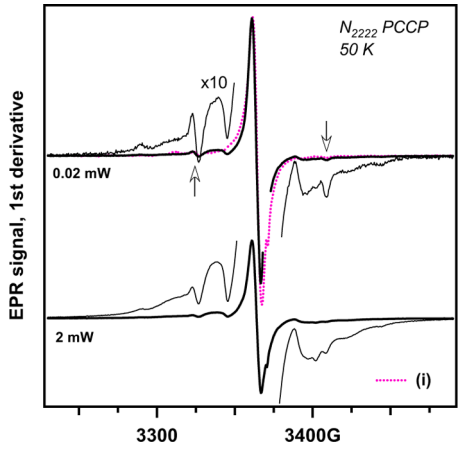

Figure 8. As Figure 7, for irradiated crystalline N_{2222} PCCP. The doublet of resonance lines indicated by arrows is attributed to an impurity center (see the text) and the resonance lines in the wings are from the $C(-H)^{\bullet+}$ radicals derived from the tetraethylammonium cation.

PCCP[30,31] obtained at 50 K. There is a narrow, saturable line at the center, while the spectral wings indicate the presence of $C(-H)^{\bullet+}$ radicals. Warming of this sample to 200 K results in the gradual decay of the latter radicals, while the narrow line persists, suggesting that the progenitor of this resonance line is derived from the $PCCP^{-}$ anion. As seen from simulations shown in Figures 1S and 10S, $PCCP^{\bullet 2-}$, $PCCP^{\bullet}$, and cyanide loss radical ($TCCP^{\bullet -}$) all have a narrow resonance line at the center of their EPR spectra. The $TCCP^{\bullet -}$ species can be

dx.doi.org/10.1021/jp404313g | J. Phys. Chem. B 2013, 117, 7084−7094

observed in K TCCP$^{\bullet-}$, where it yields a narrow resonance line with g = 2.0048 and (ΔB_{pp} ~5.8 G, as shown in Figure 22S(a)). The anion-derived radical observed in the irradiated N_{4444} PCCP has a different g-factor (g = 2.0052) and a wider spectral envelope (ΔB_{pp} ~6.4 G), suggesting that it is not TCCP$^{\bullet-}$. There are also two features indicated by arrows in Figure 8 and Figure 22S(b) that are most clearly observed in the samples annealed at 300 K (at lower temperature, these two features are masked by the resonance lines of C(−H)$^{\bullet+}$ radicals before the thermal annealing). The same two features were observed in irradiated K TCCP and $(N_{4444})_2$ TDCP, and they seem to originate from a common (aromatic) impurity. The proton hfcc corresponding to this doublet is much greater than the one expected in either the HZ$^{\bullet}$ or HZCN$^{\bullet-}$ radicals (Figure 10S). As we have not observed the anticipated EPR signature of the Z$^{\bullet-}$ anion or HZ$^{\bullet}$ radical, we conclude that the PCCP^{-} does not fragment in its reduced state.

4.1.6. TDCP^{2-} (1,2,3-Tris(dicyanomethylene)-cyclopropanediide). $(N_{4444})_2$ TDCP[19,32] was the only polynitrile dianion examined. The EPR spectrum of the irradiated crystalline material (Figure 23S(a)) reveals a background from the C(−H)$^{\bullet+}$ radicals and a narrow, very saturable line with $\Delta B_{pp} \approx 3.2$ G that clearly originates from the TDCP$^{\bullet-}$ radical (Figure 2S). In addition to this species, there is another radical whose outer lines can be observed against the background of the C(−H)$^{\bullet+}$ radicals (indicated by the arrows in Figure 23S(a)). At 300 K, the C(−H)$^{\bullet+}$ radicals decay, and this doublet spaced by 78.5 G can be observed without interference (Figure 23S(b)). Comparison with the EPR spectra shown in Figure 11S indicates that this feature cannot originate from the corresponding H adduct, HZ$^{\bullet-}$ anion, or $HC_3Q_2^{\bullet}$ radical which all have small hfcc's in the proton (Table 6S and Figure 12S). These lines seem to belong to the same impurity center that was observed in the irradiated PCCP^{-} and TCCP$^{\bullet-}$ compounds. It appears that no reduction of the $CQ_3^{\bullet 2-}$ dianion has occurred (as was the case with the DCA^{-} anion),[9,10] as might be expected for such a strongly negatively charged species; instead, the excess electron is trapped by an aromatic impurity present in the sample.

4.2. Product Analyses of Irradiated ILs. As seen from section 4.1, there is no EPR evidence for reductive fragmentation in low-temperature radiolysis of TCAP, HCAP, and PCCP, while there is significant fragmentation in TCM and PCP. For the latter compounds, both fragmentation and protonation were observed. As protonation is considerably slowed down at low temperature, it is not clear whether the loss of the cyanide occurs in room temperature radiolysis, as the reaction is only slightly exergonic. Since TCM^{-} is a very poor H atom acceptor, it is likely to still eliminate cyanide at elevated temperature, while for PCP^{-} this matter needs to be settled by product analysis.

As was observed in section 3, collisional or electronic excitation of gas-phase TCAP^{-}, PCP^{-}, and HCAP^{-} anions causes the elimination of C_2N_2, and such reactions can occur in radiolysis. To assess the extent of the radiolytic damage, we have irradiated three ionic liquids, $P_{666,14}$ TCM, $P_{666,14}$ TCAP, and $P_{666,14}$ PCP using 2.5 MeV electrons. The IL samples were irradiated at 300 K to a total dose of 2−4 MGy that was considerably higher than the expected life cycle exposure of IL diluents (0.5 MGy),[2,9] and the dose rate was also ~10^3 greater than this rate in a practical setting. Thus, this irradiation regime is more punishing, and so it presents a stringent test for radiolytic stability.

Figure 24S shows the MS_1^{+} spectra of acetonitrile solutions of irradiated ILs, in which the ion counts from the parent cation (C^{+}) were normalized to 100%. In addition to the parent cation (C^{+}) and product/impurity cations (P^{+}), there are cluster cations with the general formula $C^{+}X^{+}A^{-}$, where X^{+} is C^{+}/P^{+}, and A^{-} is the polynitrile anion. In Figure 24S, strong signals from these C^{+} and $C^{+}{}_2A^{-}$ cations have been excluded from the plot. There are multiple impurity peaks indicated by asterisks, such as $+C_2H_5$ and $-C_2H_5$ satellite peaks around the C^{+} peak. As seen from Figure 24S, even prolonged irradiation of these ILs failed to yield product peaks that exceed the amplitude of the pre-existing impurity ions. The largest of these mass peaks correspond to the addition of detached C_6 and C_{14} arms to the parent cation. There are also (mono)cations produced by joining of the two $P_{666,14}$ cations or a $P_{666,14}$ cation with a $P_{266,14}$ fragment. The yield of such dimer species in the TCAP^{-} and PCP^{-} compounds is reduced, suggesting that these anions serve as quenchers for electronically excited $P_{666,14}^{+}$ cations. Overall, these mass spectra suggest that radiolytic damage to $P_{666,14}^{+}$ cations in the ILs composed of the polynitrile anions is quite negligible, and radiolytic degradation is primarily by decomposition of the constituting anions.

Turning to the MS_1^{-} spectra for $P_{666,14}$ TCM given in Figure 25S(a) and summarized in Table 3, these spectra validate the mechanistic conclusion reached in section 4.1.1, as there are multiple anions incorporating the released $(CN)_2C$ group. In particular, the $C_2(CN)_x^{-}$ anion family (x = 3, 5, and 6) is observed, with the x = 5 species yielding the greatest contribution, and there are also $C_2(CN)_5R^{-}$ anions, where R is fragments of the aliphatic arms of the cation. The NQ_2^{-} and

Table 3. Mass Peaks and Relative Yields of Product Anions in the Irradiated IL Samples (3 MGy) As Determined Using ESI MS_1^{-}

anion	m/z MS_1^{-}	%
1. $P_{666,14}$ TCM		
QCCN	102.4	10
QCCCN	114.5	13
NQ_2	141.8	25
$C_2(CN)_5$	154.8	100[a]
$C_2(CN)_6$	180.8	28
$C_2(CN)_5-C_4H_9$	212.2	83
$C_2(CN)_5-C_5H_{11}$	226.1	46
?	234.9	45
$C_2(CN)_5-C_6H_{13}$	238.9	37
2. $P_{666,14}$ TCAP		
QNCHCN	117.4	1.4
$N_2(CN)_4$	132.4	3.1
NQ_2[b]	142.4	100[a]
$QNC(CN)CONH_2$	160.5	57
$C_2(CN)_6$	180.6	2.4
$N[C(CN)_2C(CN)]_2$	194.7	2.9
$(CN)_8$	208.8	3
3. $P_{666,14}$ PCP		
QCCCN	114.4	*b*
$NCCQ_2$[b]	166.2	100[a]
$C_2(CN)_6$	180.3	0.3
CQ_3	204.3	0.3

[a]Taken for 100%. [b]Parent anion. [c]Fragment of the parent anion formed w/o radiolysis.

dx.doi.org/10.1021/jp404313g | J. Phys. Chem. B 2013, 117, 7084−7094

$QCCCN^-$ anions[32] also occur, suggesting extensive secondary chemistry of the fragment radicals.[33]

According to Figure 25S(b) and Table 3, $TCAP^-$ also appears to be unsuitable. There is significant hydrolytic damage[21] to one of the cyano groups that is transformed to the carboxamide group (m/z −160.5). Upon collisional excitation, this product anion fragments to $QNCHCN^-$ and HNCO. Such hydrolysis occurs by a reaction of a chemically unstable precursor with the moisture present in organic solvents used to prepare samples for NMR and MS analyses. In the corresponding ^{13}C NMR spectra (Figure 26S), there are products with chemical shifts of 158.8 and 165.6 ppm that are typical for carbonyl and isocyanide carbons, and there is also a resonance at 94.8 ppm that belongs to carbon-1 (Scheme 1) in an $QNC(CN)CONH_2^-$ compound (our DFT estimates for carbon-13 shifts in this product anion are 159.3 and 97.7 ppm, respectively). In addition to this product, there are several minor products indicating C_2N_2 loss, N−C bond cleavage, and cross reactions of the released fragments (Table 3).

In contrast to $TCAP^-$, only two minor products, that is $C_2(CN)_6^{\bullet-}$ and $CQ_3^{\bullet-}$, appear in the mass spectra of irradiated $P_{666,14}$ PCP (Figure 25S(c) and Table 3). The ^{13}C NMR spectrum shown in Figure 27S also indicates the low yield of radiolytic products. The only strong resonance signal (at 54.7 ppm) is from a product that accounts for <5% conversion of carbon-1 in PCP^- to this product after 1.85 MGy irradiation; this is equivalent to the loss of just 1.5% of the PCP^- anions over the entire lifecycle of the IL diluent. Thus, contrary to low-temperature radiolysis of PCP^- that indicates significant cyanide loss, room temperature radiolysis does not result in such elimination. As was suggested above, the likely rationale for this behavior is that, at 300 K, the protonation of $PCP^{\bullet 2-}$ occurs faster than the elimination of cyanide.

5. CONCLUDING REMARKS

The development of IL diluents for nuclear separations is hampered by the dearth of constituent anions that combine high hydrophobicity, extremely low proton affinity, and high radiation resistance. The main result of this study is that polynitrile anions can meet this outstanding challenge. Only the two simplest representatives of this large class of anions containing only carbon and nitrogen, dicyanamide, and tricyanomethanide have been studied systematically by the IL community; e.g., refs 16−18 and 34. Methods for synthesis of the corresponding polynitrile ILs have been developed, and their radiation resistance has been assessed.

By their nature, these polynitrile anions are resistant to *oxidative* fragmentation, which is the leading cause for irreversible loss of organic anions in radiolysis of ILs. We established that *the reduced forms of some of these polynitrile anions are also stable*: the corresponding radical dianions may undergo protonation, but there is generally no elimination of cyanide, in contrast to halogenated anions, for which the release of halide is a common occurrence. Two exceptions to this rule have been found: tricyanomethanide that eliminates cyanide at any temperature, and 1,1,2,3,3-pentacyanopropenide (PCP^-, Scheme 1) that eliminates cyanide at low temperature, but becomes rapidly protonated at 300 K, thereby avoiding cyanide loss.

The "weak spot" of the complex polynitrile anions is their dissociation (with the elimination of cyanogen) in radiolytically generated electronically excited states. Nevertheless, PCP^- was shown to be resistant to this kind of fragmentation as well. It is likely that there are other such examples, such as pentacyanocyclopentanide ($PCCP^-$, Scheme 1) which lacks vicinal nitrile groups that are conducive to the loss of cyanogen. As such anions are more exotic than PCP^-, which is both exceptionally robust and easy to synthesize,[20b] further exploration of polynitrile anions requires a dedicated synthetic effort.

We urge systematic exploration of such polynitrile anion based ILs, as it can complement the ongoing studies of ILs consisting of fluorinated anions. Regarding their suggested use as diluents for metal separations, PCP^- and $PCCP^-$ coordinate d- and f-block metal ions only weakly, which suggests minimal interference of such complexation with nuclear separations.[30,31] We caution that our assessment of radiation stability has been carried out in neat IL, whereas IL diluents are exposed to strong (oxidizing) acids. As the cyanide groups can be hydrolyzed, care needs to be exercised to quantify such damage in a particular setting. Such concerns are not specific to polynitrile anions; indeed, many fluorinated anions, such as BF_4^- and PF_6^-, are prone to rapid hydrolytic cleavage.[35]

Besides this specific application, polynitrile ILs can be used in other situations where halogen-free composition is desired such as in lubricants, where tribochemical damage causes fluoride release that compromises lube performance on metal surfaces.[36] As the redox reactions of polynitrile anions yields stable charged species, these can be used as charge carriers in electrochemical (e.g., lithium battery) and photoelectrochemical (e.g., solar cell) applications.[18,36,37]

We hope that this study will ignite interest in this heretofore underexplored class of ionic liquids.

■ ASSOCIATED CONTENT

Supporting Information

A PDF file containing a list of abbreviations, synthetic procedures (Section 1S), Tables 1S−6S, and Figures 1S−27S with captions, including the experimental and simulated EPR spectra, NMR and MS data, and DFT calculations. This material is available free of charge via the Internet at http://pubs.acs.org.

■ AUTHOR INFORMATION

Corresponding Author

*Tel.: (630) 252-9516. E-mail: shkrob@anl.gov.

Notes

The authors declare no competing financial interest.

■ ACKNOWLEDGMENTS

I.A.S. thanks K. Quigley and J. Muntean for technical support, J. Schlueter and M. Johnson for helpful discussions, and Professor Joel S. Miller (University of Utah) for his helpful insights and a generous gift of polynitrile compounds. The work at Argonne and Brookhaven was supported by the US-DOE Office of Science, Division of Chemical Sciences, Geosciences and Biosciences, under contracts Nos. DE-AC02-06CH11357 and DE-AC02-98CH10886, respectively. Programmatic support via a DOE SISGR grant "An Integrated Basic Research Program for Advanced Nuclear Energy Separations Systems Based on Ionic Liquids" is gratefully acknowledged.

■ REFERENCES

(1) Hallett, J. P.; Welton, T. Room-Temperature Ionic Liquids: Solvents for Synthesis and Catalysis. 2. *Chem. Rev.* **2011**, *111*, 3508−

3576. Welton, T. Room-Temperature Ionic Liquids. Solvents for Synthesis and Catalysis. *Chem. Rev.* **1999**, *99*, 2071−2083. Plechkova, N. V.; Seddon, K. R. Applications of Ionic Liquids in the Chemical Industry. *Chem. Soc. Rev.* **2008**, *37*, 123−150. Smiglak, M.; Metlen, A.; Rogers, R. D. The Second Evolution of Ionic Liquids: From Solvents and Separations to Advanced Materials—Energetic Examples from the Ionic Liquid Cookbook. *Acc. Chem. Res.* **2007**, *40*, 1182−1192. Parvulescu, V. I.; Hardacre, C. Catalysis in Ionic Lquids. *Chem. Rev.* **2007**, *107*, 2615−2665. Binnemans, K. Lanthanides and Actinides in Ionic Liquids. *Chem. Rev.* **2007**, *107*, 2592−2614.

(2) Sun, X. Q.; Luo, H. M.; Dai, S. Ionic Liquids-Based Extraction: A Promising Strategy for the Advanced Nuclear Fuel Cycle. *Chem. Rev.* **2012**, *112*, 2100−2128. Wishart, J. F.; Shkrob, I. A. The Radiation Chemistry of Ionic Liquids and its Implications For their Use in Nuclear Fuel Processing. In *Ionic Liquids: From Knowledge to Application*; Plechkova, N. V., Rogers, R. D., Seddon, K. R., Eds.; American Chemical Society: Washington, DC, 2009; pp 119−134.

(3) Berthon, L.; Nikitenko, S. I.; Bisel, I.; Berthon, C.; Faucon, M.; Saucerotte, B.; Zorz, N.; Moisy, P. Influence of Gamma Irradiation on Hydrophobic Room-Temperature Ionic Liquids $[BuMeIm]PF_6$ and $[BuMeIm](CF_3SO_2)_2N$. *Dalton Trans.* **2006**, 2526−2534. Le Rouzo, G.; Lamouroux, C.; Dauvois, V.; Dannoux, A.; Legand, S.; Durand, D.; Moisy, P.; Moutiers, G. Anion Effect on Radiochemical Stability of Room-Temperature Ionic Liquids under Gamma Irradiation. *Dalton Trans.* **2009**, 6175−6184. Allen, D.; Baston, G.; Bradley, A. E.; Gorman, T.; Haile, A.; Hamblett, I.; Haatter, J. E.; Healey, M. J. F.; Hodgson, B.; Lewin, R.; et al. An Investigation of the Radiochemical Stability of Ionic Liquids. *Green Chem.* **2002**, *4*, 152−158.

(4) Yuan, L. Y.; Xu, C.; Peng, J.; Xu, L.; Zhai, M. L.; Li, J. Q.; Wei, G. S.; Shen, X. H. Identification of the Radiolytic Product of Hydrophobic Ionic Liquid $[C_4mim][NTf_2]$ During Removal of Sr^{2+} from Aqueous Solution. *Dalton Trans.* **2009**, 7873−7875. Yuan, L. Y.; Peng, J.; Xu, L.; Zhai, M. L.; Li, J. Q.; Wei, G. S. Radiation Effects on Hydrophobic Ionic Liquid $[C_4mim][NTf_2]$ During Extraction of Strontium Ions. *J. Phys. Chem. B* **2009**, *113*, 8948−8952. Yuan, L. Y.; Peng, J.; Xu, L.; Zhai, M. L.; Li, J. Q.; Wei, G. S. Influence of Gamma-Radiation on the Ionic Liquid $[C_4mim][PF_6]$ During Extraction of Strontium Ions. *Dalton Trans.* **2008**, 6358−6360.

(5) Berthon, L.; Chabronnel, M.-C. Tadiolysis of Solvents Used in Nuclear Fuel Reprocessing. In *Ion Exchange and Solvent Extraction, A Series of Advances*; Moyer, B. A., Ed.; CRC Press: Roca Baton, FL, 2010; Vol. *19*, pp 429−513.

(6) Marin, T. W.; Shkrob, I. A.; Dietz, M. L. Hydrogen-Bonding Interactions and Protic Equilibria in Room-Temperature Ionic Liquids Containing Crown Ethers. *J. Phys. Chem. B* **2011**, *115*, 3912−3918.

(7) Shkrob, I. A.; Marin, T. W.; Chemerisov, S. D.; Wishart, J. F. Radiation Induced Redox Reactions and Fragmentation of Constituent Ions in Ionic Liquids. 1. Anions. *J. Phys. Chem. B* **2011**, *115*, 3872−3888.

(8) Shkrob, I. A.; Marin, T. W.; Chemerisov, S. D.; Hatcher, J. L.; Wishart, J. F. Radiation Induced Redox Reactions and Fragmentation of Constituent Ions in Ionic Liquids. 2. Imidazolium Cations. *J. Phys. Chem. B* **2011**, *115*, 3889−3902.

(9) Shkrob, I. A.; Wishart, J. F. Free Radical Chemistry in Room-Temperature Ionic Liquids. In *Encyclopedia of Radicals in Chemistry, Biology and Materials*; Chatgilialoglu, C., Studer, A., Eds.; John Wiley & Sons, Ltd.: Chichester, UK, 2012; pp 433−448.

(10) Shkrob, I. A.; Chemerisov, S. D.; Wishart, J. F. The Initial Stages of Radiation Damage in Ionic Liquids and Ionic Liquid-Based Extraction Systems. *J. Phys. Chem. B* **2007**, *111*, 11786−11793.

(11) Shkrob, I. A.; Wishart, J. F. Charge Trapping in Imidazolium Ionic Liquids. *J. Phys. Chem. B* **2009**, *113*, 5582−5592.

(12) Shkrob, I. A.; Marin, T. W.; Chemerisov, S. D.; Hatcher, J. L.; Wishart, J. F. Toward Radiation-Resistant Ionic Liquids. Radiation Stability of Sulfonyl Imide Anions. *J. Phys. Chem. B* **2012**, *116*, 9043−9055.

(13) Avelar, A.; Tham, F. S.; Reed, C. A. Superacidity of Boron Acids $H_2(B_{12}X_{12})$ (X=Cl, Br). *Angew. Chem., Int. Ed.* **2009**, *48*, 3491−3493. Larsen, A. S.; Holbrey, J. D.; Tham, F. S.; Reed, C. A. Designing Ionic Liquids: Imidazolium Melts with Inert Carborane Anions. *J. Am. Chem. Soc.* **2000**, *122*, 7264−7272.

(14) Kutt, A.; Rodima, T.; Saame, J.; Raamat, E.; Maemets, V.; Kaljurand, I.; Koppel, I. A.; Garlyauskayte, R. Yu.; Yagupolskii, Yu. L.; Yagupolskii, L. M.; Bernhardt, E.; Willner, H.; Leito, I. Equilibrium Acidities of Superacids. *J. Org. Chem.* **2011**, *76*, 391−395.

(15) Kozisek, J.; Dunaj-Jurco, M.; Grobe, U.; Kohler, H. Structure of Pyridinium 1,1,3,3-Tetracyano-2-Azapropenide. *Acta Crystallogr.* **1990**, *C46*, 2422−2424.

(16) MacFarlane, D. R.; Forsyth, S. A.; Golding, J.; Deacon, G. B. Ionic Liquids Based on Imidazolium, Ammonium and Pyrrolidinium Salts of the Dicyanamide Anion. *Green Chem.* **2002**, *4*, 444−448.

(17) Forsyth, S. A.; Batten, S. R.; Dai, Q.; MacFarlane, D. R. Ionic Liquids Based on Imidazolium and Pyrrolidinium Salts of the Tricyanomethanide Anion. *Aust. J. Chem.* **2004**, *57*, 121−124.

(18) Marszalek, M.; Fei, Z. F.; Zhu, D. R.; Scopelliti, R.; Dyson, P. J.; Zakeeruddin, S. M.; Gratzel, M. Application of Ionic Liquids Containing Tricyanomethanide [C(CN)(3)](-) or Tetracyanoborate $[B(CN)_4]^-$ Anions in Dye-Sensitized Solar Cells. *Inorg. Chem.* **2011**, *50*, 11561−11567.

(19) Gao, H. X.; Zeng, Z.; Twamley, B.; Shreeve, J. M. Polycyano-Anion-Based Energetic Salts. *Chem.—Eur. J.* **2008**, *14*, 1282−1290.

(20) (a) Middleton, W. J.; Little, E. L.; Coffman, D. D.; Engelhardt, V. A. Cyanocarbon Chemistry. V. Cyanocarbon Acids and their Salts. *J. Am. Chem. Soc.* **1958**, *80*, 2795−2806. (b) Middleton, W. J.; Wiley, D. W. Tetramethylammonium 1,1,2,3,3-Pentacyanopropenide in. *Org. Synth. Collect. Vol.* **1973**, *5*, 1013.

(21) Biehler, J.-M.; Perchais, J.; Fleury, J.-P. Azométhines à Substituants Électroattracteurs. I. Synthèse et Configuration de Dérivés Isonitrosomaloniques Sulfonylés et Acylés. *Bull. Soc. Chim.* **1971**, 2711−2716. Perchais, J.; Fleury, J.-P. Azométhines à Substituants Électroattracteurs. III. Action des Nucleophiles sur L'O-Para-Toluenesulfonylisonitrosomalodinitrile. *Tetrahedron* **1974**, *30*, 999−1009.

(22) Dhar, D. N. The Chemistry of Tetracyanoethylene. *Chem. Rev.* **1967**, *67*, 611−622.

(23) Sisak, D.; McCusker, L. B.; Buckl, A.; Wuitschik, G.; Wu, Y.-L.; Schweizer, W. B.; Dunitz, J. D. The Search for Tricyanomethane (Cyanoform). *Chem.—Eur. J.* **2010**, *16*, 7224−7230.

(24) Kaba, R. A.; Ingold, K. U. Kinetic Applications of Electron Paramagnetic Resonance Spectroscopy. XXIII. Cyanomethyl Radicals. *J. Am. Chem. Soc.* **1976**, *98*, 523−526.

(25) Eberson, L.; McCullough, J. Generation of Tricyanomethyl Spin Adducts of α-Phenyl-N-*Tert*-Butylnitrone (PBN) via Non-Conventional Mechanisms. *J. Chem. Soc., Perkin Trans. 2* **1998**, 49−58.

(26) Riegel, P. H.; Fraenkel, G. K. Spin Density Distribution in Nitrile Anion Radicals. *J. Chem. Phys.* **1962**, *37*, 2795−2810.

(27) Becke, A. D. Density-Functional Exchange-Energy Approximation with Correct Asymptotic Behavior. *Phys. Rev. A* **1988**, *38*, 3098−3100. Lee, C.; Yang, W.; Parr, R. G. Development of the Colle-Salvetti Correlation-Energy Formula into a Functional of the Electron Density. *Phys. Rev. B* **1988**, *37*, 785−789.

(28) Frisch, M. J.; Trucks, G. W.; Schlegel, H. B.; Scuseria, G. E.; Robb, M. A.; Cheeseman, V. G.; Montgomery, J. A., Jr.; Vreven, K. N.; Kudin, J. C.; Burant, J. C.; et al. *Gaussian 03, rev. C.02*; Gaussian, Inc.: Wallingford, CT, 2004.

(29) Chen, X.; Syrstad, E. A.; Turecek. Direct Observation of the Forbidden Hydrogen Atom Adduct to Acetonitrile: A Neutralization−Reionization Mass Spectrometric and CCSD(T) ab Initio/RRKM Study. *J. Phys. Chem. A* **2004**, *108*, 4163−4173. Chandra, H.; Symons, M. C. R. Electron-addition and electron-loss pathways for cyanoalkanes. *J. Chem. Soc., Faraday Trans. 1* **1988**, *84*, 3401−3412.

(30) Less, R. J.; Wilson, T. C.; McPartlin, M.; Wood, P. T.; Wright, D. S. Transition Metal Complexes of the Pentacyanocyclopentadienide Anion. *Chem. Commun.* **2011**, *47*, 10007−10009. Less, R. J.; Guan, B.; Muresan, N. M.; McPartlin, M.; Reisner, E.; Wilson, T. C.; Wright, D. S. Group 11 Complexes Containing the $[C_5(CN)_5]^-$ Ligand; 'Coordination-Analogues' of Molecular Organometallic Systems. *Dalton Trans.* **2012**, *41*, 5919−5924.

(31) Richardson, C.; Reed, C. A. Exploration of the Pentacyanocyclo-pentadienide Ion, $C_5(CN)_5^-$, as a Weakly Coordinating Anion and Potential Superacid Conjugate Base. Silylation and Protonation. *Chem. Commun.* **2004**, 706−707.
(32) Thétiot, F.; Triki, S.; Sala-Pala, J.; Golhen, S. The Cyanocarbanion $(C[C(CN)_2]_3)^{2-}$ as Monodentate Ligand: Synthesis, Structure and Magnetic Properties of $[Mn_2(bpym)_3(tcpd)_2(H_2O)_2]$ ($tcpd^{2-}$ = $(C[C(CN)_2]_3)^{2-}$ and bpym = 2,2′-bipyrimidine). *Inorg. Chem. Acta* **2005**, *358*, 3277−3282.
(33) Chen, M.; Liu, J.; Dang, L.; Zhang, Q.; Au, C. T. A Density Functional Study on Nitrogen-Doped Carbon Clusters $C_nN_3^-$ (n =1−8). *J. Chem. Phys.* **2004**, *121*, 11661−11667. Sun, S.; Cao, Y.; Sun, Z.; Tang, Z.; Zheng, L. Experimental and Theoretical Studies on Carbon−Nitrogen Clusters $C_{2n}N_7^-$. *J. Phys. Chem. A* **2006**, *110*, 8064−8072.
(34) Weidinger, D.; Houchins, C.; Owrutsky, J. C. Vibrational Dynamics of Tricyanomethanide. *Chem. Phys. Lett.* **2012**, *525*−*26*, 60−63.
(35) Freire, M. G.; Neves, C.; Marrucho, I. M.; Coutinho, J. A. P.; Fernandes, A. M. Hydrolysis of Tetrafluoroborate and Hexafluorophosphate Counter Ions in Imidazolium-Based Ionic Liquids. *J. Phys. Chem. A* **2010**, *114*, 3744−3749.
(36) Minami, I.; Inada, T.; Okada, Y. Tribological Properties of Halogen-Free Ionic Liquids. *J. Eng. Tribol.* **2012**, *226*, 891−902.
(37) Raabe, I.; Wagner, K.; Guttsche, K.; Wang, M.; Grätzel, M.; Santiso-Quiñones, G.; Krossing, I. Tetraalkylammonium Salts of Weakly Coordinating Aluminates: Ionic Liquids, Materials for Electrochemical Applications and Useful Compounds for Anion Investigation. *Chem.—Eur. J.* **2009**, *15*, 1966−1976.